Environ Earth Sci
DOI 10.1007/s00254-008-1676-3

ORIGINAL ARTICLE

Environmental study for pollution in the area of Megalopolis power plant (Peloponnesos, Greece)

Apostolos Sarris · Eleni Kokinou · Eleni Aidona · Nikolaos Kallithrakas-Kontos · Pavlos Koulouridakis · Georgia Kakoulaki · Kassiani Droulia · Ourania Damianovits

Received: 20 May 2008 / Accepted: 26 November 2008

Abstract The main purpose of the present study is to investigate the suitability of magnetic properties in correlation to geochemical measurements as a pollution-monitoring tool and study the metal transmission factors in an area around a major local source, namely a lignite-burning power plant. Surface soil samples were collected in the wide area of the power plant of Megalopolis (Peloponnesos, Greece). The magnetic susceptibility and other magnetic properties of the surface soils were originally measured and mapped. Loci of high values of magnetic susceptibility within the study area gave rise to further analyze the soil samples for metal concentrations. GIS techniques were used for mapping all the chemical constituent concentrations and the magnetic measurements on the various topographic and geological features of the area. Maps were created through interpolation algorithms indicating the spatial distribution of the above measurements. Spatial tools and statistical analysis through the calculation of Pearson's coefficients proved the correlation between magnetic properties, metal concentrations and the terrain attributes (especially the geological structure and the wind currents) of the region.

Keywords Magnetic susceptibility · Metals · Power plant · GIS mapping · Megalopolis (Greece)

A. Sarris · G. Kakoulaki
Laboratory of Geophysical–Satellite Remote Sensing & Archaeo-environment, Institute for Mediterranean Studies, Foundation for Research and Technology—Hellas, P.O. Box 119, 74100 Rethymnon, Crete, Greece
e-mail: asaris@ret.forthnet.gr

E. Kokinou (✉) · K. Droulia · O. Damianovits
Laboratory of Geophysics and Seismology, Department of Natural Resources and Environment, Technological Educational Institute Crete, 3 Romanou Str. Chalepa, 73133 Chania, Crete, Greece
e-mail: ekokinou@chania.teicrete.gr

E. Aidona
Department of Geophysics, Aristotle University of Thessaloniki, 54006 Thessaloniki, Greece
e-mail: aidona@geo.auth.gr

N. Kallithrakas-Kontos · P. Koulouridakis
Analytical and Environmental Chemistry Lab, Technical University of Crete, Chania, Crete, Greece
e-mail: kalli@mred.tuc.gr

P. Koulouridakis
e-mail: pkoul@mred.tuc.gr

Introduction

Magnetic susceptibility is a measure of how easy a material can be magnetized (Thompson and Oldfield 1986) and is defined by the quantities of volume susceptibility k (dimensionless) and mass-specific susceptibility χ. In the last two decades, magnetic susceptibility is examined in terms of its ability to be used as a successful pollution-monitoring tool. Hansen et al. (1981) indicated that chromium manganese, cobalt, nickel, copper, zinc and beryllium are all significantly enriched in the 'magnetic' fraction of coal fly-ash. Beckwith et al. (1984) identified pollution sources in urban drainage systems using magnetic methods. Petrovský and Ellwood (1999) reviewed the application of magnetic susceptibility measurements in various ecosystems. Lately, more researchers investigate the usage of magnetic susceptibility as a tool for contaminated top soils and sediments (Scholger 1998; Bityukova et al. 1999; Petrovsky et al. 2001; Boyko et al. 2004;

Kokinou et al. 2008). The relationship between magnetic oxides and heavy metals in urban airborne particulate materials such as metallurgical dust, fly ashes and cement dust has been intensively studied (Strzyszcz et al. 1996; Goluchowska 2001; Schmidt et al. 2005). In the last years, the study of the pollution loads around major local source-coal-burning power plants attracts the attention of research (Kapička et al. 1999; Sharma and Tripathi 2008). Accumulation of anthropogenic ferromagnetic particles originating during high-temperature combustion of fuels (Vassilev 1992; Dekkers and Pietersen 1992) results in significant enhancement of top soil magnetic susceptibility. Fly ashes from coal combustion and dusts from various industrial processes contain very high level of trace metals. Therefore, the concentration of trace metals in surface soils could be affected by the deposition of such industrial emissions. For these reasons, magnetic properties in combination with geochemical analyses are used in the present study to monitor the environmental pollution and study the metal transmission factors.

Magnetic particles are usually deposited downwind from the industrial units on the surface of soils, streets, buildings and trees. According to Flanders (1994) and Hoffmann et al. (1999), the amount of settled magnetic material decreases with distance from the emission source. Fly ashes with significant portion of magnetic minerals (Flanders 1994, 1999) are produced by industrial processes such as combustion of fossil fuel; they are transported through atmospheric pathways and deposited on the ground. In soils, such particles penetrate downwards and accumulate in top layers and their increased concentration can be easily detected using surface magnetic measurements (e.g., Lecoanet et al. 1999).

Scope of this paper is the study of the environmental pollution caused by the activities of a power plant, located in Megalopoli's basin (Peloponnessos), through the employment of magnetic susceptibility methods and geochemical analysis. The relation among the magnetic properties of the soils, their chemical constituents and the geomorphologic characteristics of the region is examined. The study takes into account the absolute lack of similar works in the geographic region of Greece and the case of a lignite power plant, which usually is responsible for creating high levels of pollution (Riga-Karandinos and Karandinos 1998; Sukumar and Subramanian 2003; Zeneli et al. 2008) in its surrounding region. In most studies, a significant correlation between magnetic susceptibility and heavy metal content in soils was found (e.g., Heller et al. 1998; Dearing et al. 2001; Lecoanet et al. 2001; Hanesch et al. 2003; Jordanova et al. 2003). In the context of the present study, the relation of the magnetic properties with a variety of metals is also investigated.

The environment of the study area

The basin of Megalopolis is located at the NW section of Arkadia Prefecture at the center of Peloponnesos (Fig. 1), having an elliptical shape whose long axis has a direction of NNW–SSE and length 18 km. It is enclosed by the mountains of Menalo (37°39′N, 22°13′E), Lykaion (37°27′N, 21°58′E) and Taygetos (36°57′N, 22°21′E) covering a total area of 180 km^2 at an average altitude of 410 m above the sea level. The lignite ores cover a total area of 40,000 m^2. The town of Megalopolis is at a distance of 200 km from Athens and 35 km from Tripoli. The area around Megalopolis consists of two municipalities and 43 communities having a population of 8,657 people.

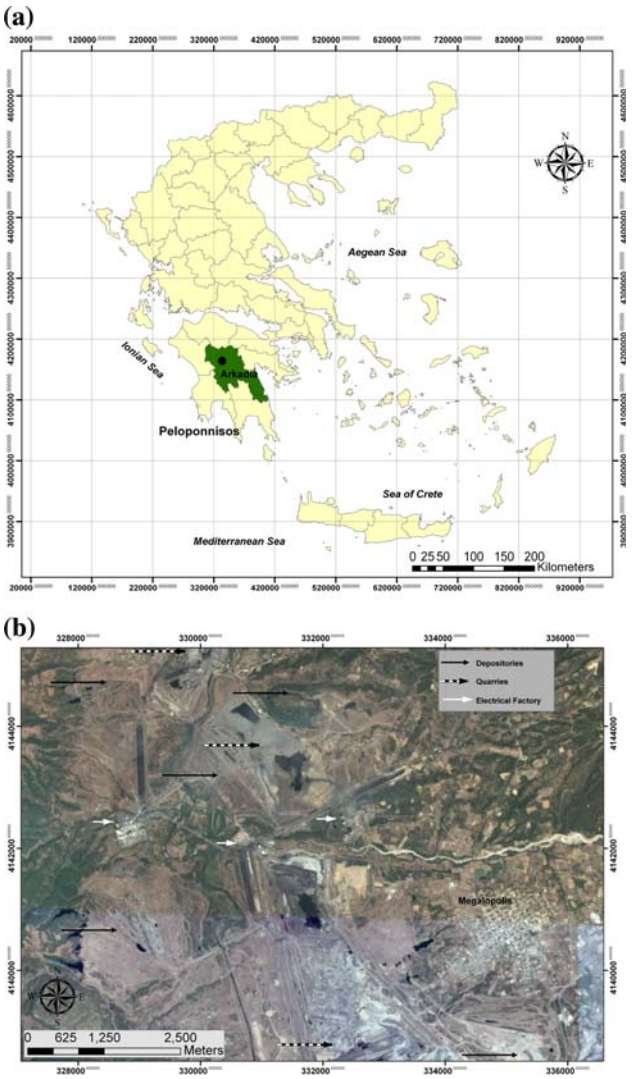

Fig. 1 (**a**) The Prefecture of Arkadia and (**b**) the location of the Megalopolis power plant (*left*). Satellite imagery from Google Earth showing the wider area of interest (*right*). The town of Megalopolis (central east side of the map), the power plant and the mines are clearly shown in the image

The climate of Megalopolis is a transient-type Mediterranean to continental (category Csa according to Koppen classification scheme). It is characterized from relatively high seasonal and daily fluctuations of the temperature and high humidity during the whole year. The main volume of rainfalls is limited in the half-year period of October to March.

The Megalopoli's basin comprises an almost flat area with slopes mainly ranging between 0 and 25%, showing an extended drainage network (Fig. 2). The softness and horizontality of the geological layers contribute basically in the configuration of the low morphology of the region, consisting mainly of round hills separated with narrow streams. The high-order branches of the drainage network are generally oriented NW–SE. The River Alfeios with its tributaries (such as Xerila, Geoudani, Elissona, a.o.) is naturally carrying away the rain waters from the valley, through a narrow gorge at the NW corner of the valley. Small canyons are also formed at the edges of the basin, having a depth of about 10 m. The lowest outlet of the valley is toward the straights of Karytaina.

The Megalopoli's basin constitutes a tectonic graben, which was created between upper Miocene and lower Pliocene (Fountoulis 2000). This tectonic graben is mainly filled by lacustrine and fluvial sediments of Holocene, Pleistocene and Neogene-Upper Pliocene (Fig. 3), which were sampled in the context of the present study. The rocks, which surrounded the basin, belong to Pindos zone and mainly consist of Jurassic limestones, crystalic schists with cherts and light-colored limestones. The territories situated on either side of the drainage network are alluvial deposits, consisting of unconsolidated clay–sandy materials, gravels and cobbies at the river and torrent beds, as well as small terraces. Additional silt, loam with scree and loose conglomerates are situated at the northeastern part of the study area. The majority of the basin's interior consists of Pleistocene sediments, comprising alterations of marls, clays, sands, lignite beds and loose conglomerates of

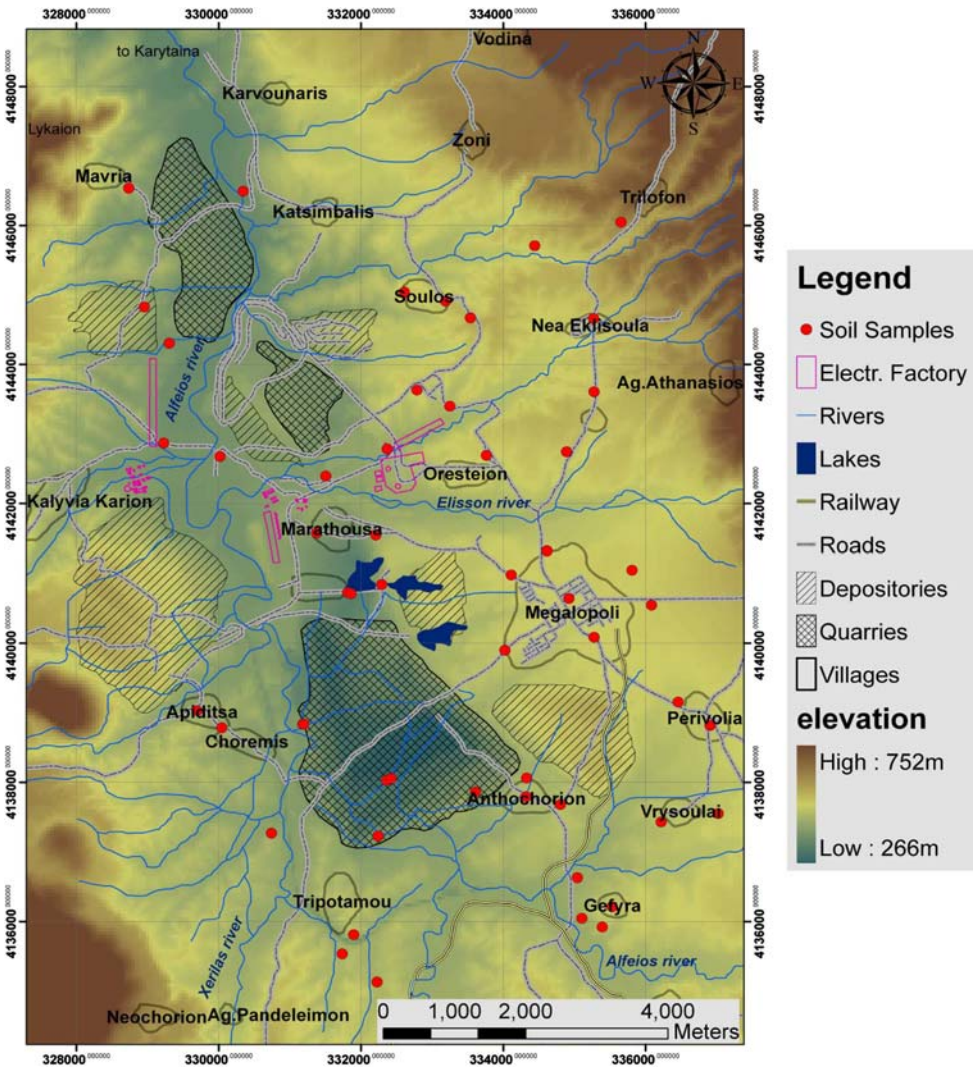

Fig. 2 Topography map of the region around the power plant of Megalopolis showing the location of the town of Megalopolis, the installations of the power plant, the location of the quarries and depositories

fluvial and lacustrine facies. The lignite-bearing beds are wedged out toward the basin margins where fluvial deposits prevail. Neogene sediments of upper Pliocene (Trilofon formation) are indicated at the northeastern part of the study area. The Trilofon formation consists of clays, marls of lacustrine facies, as well as fluvial deposits of clays, marls, sands and slightly cohesive cross-bedded conglomerates. Formations such as the Paleocene Flysch transition bed, the upper Cretaceous platy to bedded multicolored limestones and the Jurassic to lower Cretaceous chert series with members of disrupted ophiolithic volcanic series, are locally indicated in the eastern, northern and western margins of the Megalopoli's basin.

The surface exploitation for the digging of lignite still causes important changes in the geomorphology. Up to now, about 27 km^2 have been expropriated and about 13 km^2 more are expected to be expropriated in the future, most of which involves cultivation fields, pasture lands and oak forests with direct consequences in the real estate and rural economy of the region. The surface exploitation has destroyed the ground surface and vegetation, leaving deserted regions fully excavated with irregular hills and elevations from depositions of barren, marshes and lakes. Roughly, the lignite fields occupy an area of 20 km^2, whereas 8.5 km^2 is covered by the exterior depositions of barren. The rest 11.5 km^2 is occupied by the deposits of lignite, road network, dams, building installations, etc.

Methodology

Site description and sampling

The lignite-burning power plant (Fig. 4) of the Hellenic Public Power Corporation (DEI) opened in 1969. The Megalopolis power plant consists of three units, the first two (125 MW) started operating in 1970 and the third (300 MW) in 1975. The power plant itself covers an area of 0.2–0.3 km^2. In the vicinity of the power plant, three lignite mines are established in an area of 20 km^2 and produce approximately 15 million tons of lignite per year. The Megalopolis Lignite Centre comprises three open-cast

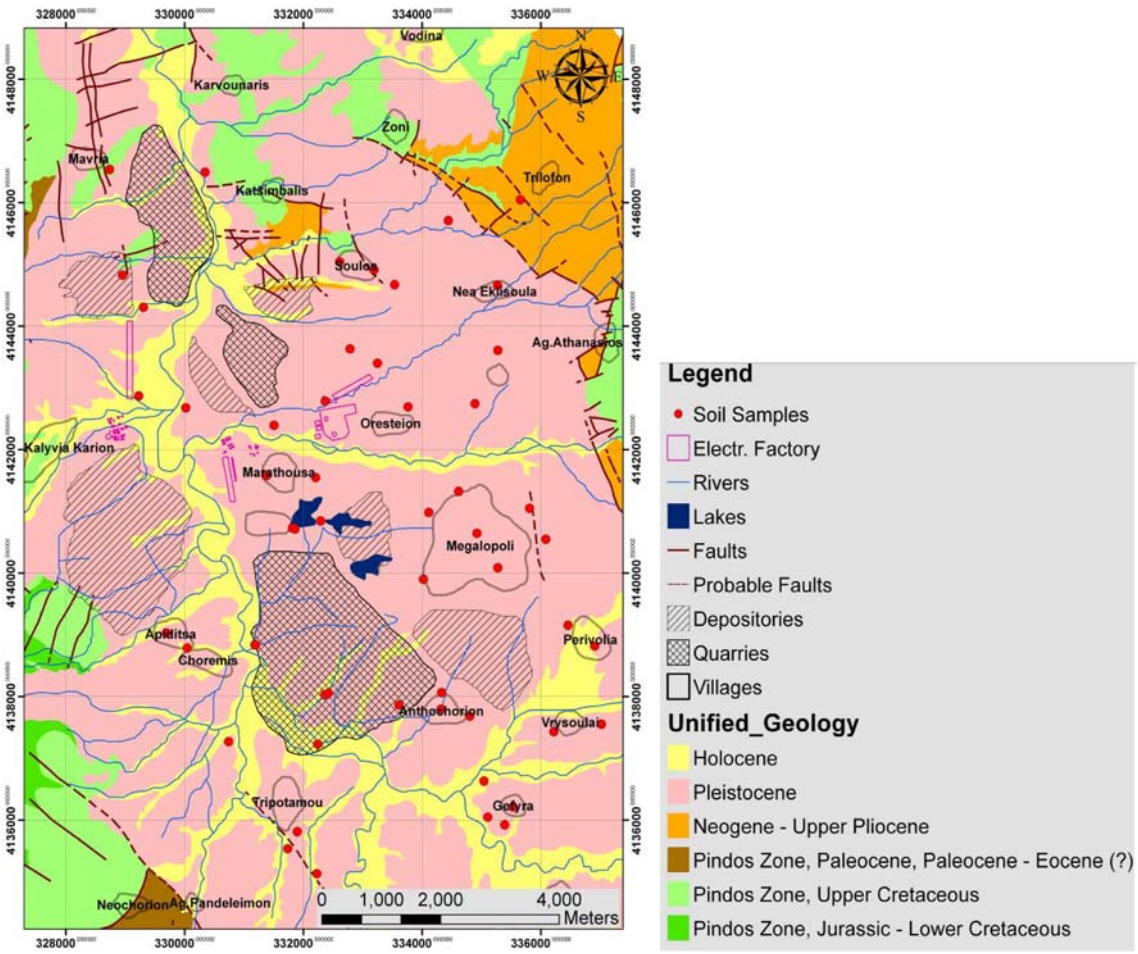

Fig. 3 Geological map of Megalopolis, produced through a generalization of the corresponding map of the Institute for Geological and Mineral Exploration of Greece (IGME)

mines (Fig. 2): the Kyparissia mine located to the north of the complex, the Marathoussa mine located centrally and the Choremi mine at the south of the complex. Excavation of lignite is made from the surface using mainly electrically driven machinery, which is also supported by about 1,500 diesel-driven machinery and vehicles, such as propellers, chargers, hydraulic excavator machinery, vans, etc. The storage of barren materials is made in specifically selected regions, where the ash and the remains of combustion are also transported. The lignite causes pollution of environment that is created by the remains of ash and the poisonous gases that are created at the combustion process (dioxide of coal, oxide of nitrogen). The excavation of lignite in the mines also pollutes the environment from dioxide of sulphur and niter gases, which are even more serious than those originating by the combustion of hydrocarbons.

Greek lignite is a poor fossil fuel produced during the first stages of carbonization, characterized by high moisture levels (approximately 55%), ash (30% or more ash, water-free) and low heat value (960–2,030 kcal/kg) and it is mainly used as a fuel in steam electric units (http://www.worldenergy.org/wec-geis/publications). All lignite-fired power plants in Greece use the pulverized coal combustion technology, which requires a drying and pulverization process before the combustion. Every power plant is equipped with electrostatic precipitators for the separation of fly ash from the exhaust gases. Ash is removed in a wet state in every power plant and part of it is used by the cement industry and in hydroelectric dam construction as well.

Top soil sampling was performed in the study area in the beginning of November 2005 within a grid covering a total area of about 102 km^2. GPS coordinates (in WGS-84 system) were taken from each sampling site and converted in Hatt projection system to be in agreement with the available topographic data. At each site, samples were taken within a depth of 0–15 cm below the surface. Soil samples were placed in plastic containers. Each of the soil samples was mixed, air-dried, disaggregated and sieved retaining the fraction smaller than 2 mm to reduce the biasing effect of air, water and pebbles.

Magnetic measurements

In environmental magnetism, the most often used magnetic parameter is the magnetic susceptibility (χ), which is the ratio of induced (temporary) magnetization acquired by a sample in the presence of a weak magnetic field to the applied field itself. In the present study, the magnetic susceptibility of all samples was measured with the dual frequency version of sensor MS2B (Bartington Instruments). Accurate measurements of mass susceptibility were obtained in two frequencies ($f_{low} = 0.43$ kHz and $f_{high} = 4.3$ kHz).

Since our samples were of unknown density, mass-specific measurements seemed to be more appropriate than the ones based on specific volume. A sample of 10 cm^3 tightly packed manganese carbonate powder ($\chi = 99.2 \times 10^{-6}$ emu/g) was used for calibration of the instrument. The consistency of the instrument calibration was checked by measuring the susceptibility of the calibration sample in the beginning and end of the measuring session. Samples were weighted and the subsequent susceptibility measurements in both frequencies were multiplied by a factor $w_f = (10/\text{weight of sample})$ to normalize our measurements for a mass of 10 g. The contribution of the plastic container was measured for 10 pieces and the average value was subtracted from all measurements.

The magnetic behavior of many minerals varies with temperature. All magnetic minerals have a temperature point (Curie temperature) above which they become paramagnetic. So, in practice, from the shape of the temperature–susceptibility curves the presence of magnetic minerals and domains can be detected. Our samples were heated with the susceptibility temperature Bartington device up to 700°C and cooled down to room temperature to identify the main magnetic carries.

Anhysteretic remanent magnetization (ARM) and isothermal remanent magnetization (IRM) are frequently used in environmental magnetic investigations. Both of them are produced by exposing a sample to an external magnetic field. ARM is the magnetization, which acquired when a sample is subjected to a dc bias field in the presence of a decreasing alternating magnetic field. Usually, the bias field is comparable in intensity to earth's magnetic field. For low field values (up to $\sim 80\ \mu$T), ARM intensity is linear with the inducing dc bias field. For low concentrations in magnetic minerals, ARM is to a first-order approximation linear with concentration. Single domain (SD) grains have high ARM intensities per unit mass, which makes ARM an attractive proxy for the determination of SD particles.

In the present study ARM measurements were performed in 16 samples in the palaeomagnetic laboratory Gams of Leoben University in Austria, using a Walker electromagnet. The selection of the studied samples was based on their susceptibility values and their distribution in the area. That is, samples with extreme values of susceptibility (high and low), which distribute near and away from the active quarries, have been selected.

IRM is the magnetization, which acquired a sample when exposed to a strong dc magnetic field. As the intensity of the field increases, the acquired magnetization increases until the sample becomes as magnetized as its

mineralogy and the laws of thermodynamic permit. At this point, the sample is saturated. If this magnetization is measured after the applied field is removed, it is called saturation remanence, which is, by definition, equivalent to the saturation IRM (SIRM). Ferrimagnetic minerals (such as magnetite and maghemite) saturate up to 300 mT, while canted ferromagnetic minerals (such as hematite and goethite) require more than 2 T for saturation (Verosub and Roberts 1995; Dekkers 1997).

In the present study, the IRM was imparted using a pulse magnetizer and was measured on a spinner magnetometer, in the Palaeomagnetic Laboratory of the University of Thessaloniki.

Geochemical analysis

Thereinafter, geochemical analysis of the collected soil samples was performed for the measurements of metal concentrations (K, Ca, Ti, Mn, Fe, Ni, Cu, Zn, Pb, Rb, Sr, Y, Zr, Nb) in units of ppm or mg kg^{-1}. The soil samples were analyzed by energy dispersive X-ray fluorescence (EDXRF) at the Analytical and Environmental Chemistry Lab of the Technical University of Crete. In this case, a small mass of soil samples (in the range of 0.5–3 g) was put and pressed in suitable plastic holders (Chemplex XRF Sample Cups No 1340) of 3.2 cm diameter with a thin Mylar bottom (with surface density equal to 0.86 mg/cm^2). The samples were irradiated with a ^{109}Cd radioactive source to excite the K and/or L shells of the analyzed elements (the technique is not destructive). ^{109}Cd isotope emits the characteristics K X-ray lines of silver (22.1, 24.9 keV) and it is suitable for simultaneous excitation of most of the elements of the periodic system. Irradiation was done overnight (usually 24 h) to succeed adequate peak intensity.

The emitted X-rays from the analyzed soil (secondary X-rays) were detected by a PGT Si(Li) semiconductor detector (resolution 150 eV at 5.9 keV, liquid nitrogen-cooled) with the following specifications: beryllium window area 33 mm^2, thickness 13 μm, crystal active area 30 mm^2, thickness 3 mm, peak/background ratio (at 5.9 keV) 3118/1. The detector was operated under a −500 V bias voltage supplied by a TC-950A Tennelec Bias Supply unit. The detector output signal was amplified by a TC-244 Tennelec Spectroscopy Amplifier, with Coarse Gain 50, pileup correction for overlapping pulses (threshold adjustable) peaking time 12 μs (shaping time 6 μs). The X-ray-detected rate was measured by a TC-525 Tennelec Ratemeter. The amplified pulses were collected by a PCA-II Nucleus Multichannel PC card (8,192 channel acquisition memory, 1 MHz crystal-controlled, 100 MHz clock frequency, Wilkinson type, 0–8 V input Unipolar, accepting pulses 0.5–30 μs). In the present application, 2,048 channels were used.

Spectra were analyzed by the AXIL$^{(RN)}$ software package supplied by the International Atomic Energy Agency. Qualitative analysis was performed by peak energy determination after an energy calibration with four to six standard elements (or compounds) of various energies. Spectra fitting were performed after peak recognition and smooth filter background subtraction. Quantitative analysis was made by the AXIL program calibrated by numerous thick standard samples (pure metals or salts, thin and thick samples). Peak overlapping (especially many Ka–Kb cases), X-ray absorption and X-ray enhancement (by other x-ray peaks) were taken into account by the fitting procedure.

The main advantages of the EDXRF technique were the capability of direct solid sample analysis, the simultaneous detection of many elements, the possibility of determination of unexpected elements and the dynamic concentration range from ppm level up to 100%.

Statistical processing

Pearson's correlation coefficient (r_{xy}) was used to estimate the correlation between metal content and magnetic properties as well as among the magnetic properties. Initially, a scatter plot of all data pairs has been done to establish if the data indicates a linear relationship, because r_{xy} indicates the strength of a linear relationship between two variables x and y for N samples. r_{xy} is defined as

$$r_{xy} = \frac{\mathrm{Cov}(x,y)}{\sqrt{\mathrm{Var}(x)}\sqrt{\mathrm{Var}(y)}} \quad (1)$$

where the covariance Cov and the variance Var are defined as

$$\mathrm{Var}(x) = \frac{\sum (x_i - \bar{x})^2}{N-1} = \frac{SS_{xx}}{N-1} \quad (2)$$

and

$$\mathrm{Cov}(x,y) = \frac{\sum (x_i - \bar{x}) \sum (y_i - \bar{y})}{N-1} = \frac{SS_{xy}}{N-1} \quad (3)$$

Values of r, ranging from −1 to −0.75 and from 0.75 to 1, correspond to perfect-strong relation of the two variables. In case the r value lies in the ranges −0.75 to −0.5 and 0.5–0.75, it indicates a moderate relation of the two variables. Finally, r values lying in the ranges −0.5 to −0.25 and 0.25–0.5 or −0.25 to 0.25 are suggestive of a weak or no linear relation between the two variables.

GIS analysis and mapping

Digitization techniques and GIS were applied for the presentation of the spatial distribution of magnetic

susceptibility measurements and metal concentrations resulting from recent or past activities (Yerkes et al. 2007; Sarris et al. 2004; Wang and Qin 2005; Romic et al. 2007). To address the correlation between the above quantities and the geomorphologic attributes of the region, a number of maps were collected and digitized. Topographic maps of the area (scale 1:50,000) were used to extract the location of the towns, the power plant, the lignite quarries and depositories. The above information was further enriched through a generalization of the geological formations of the region available by 1:50,000 scale geological maps of the Institute of Geological and Mineral Exploration (IGME). Faults, rivers, lakes and the main and secondary roads and railway network were also digitized and fused to the Geographical Information System component of the project. The samples' location was also superimposed on the maps (Figs. 2, 3).

The digital elevation model was created by the digitization of the topographic map contours, while the cell size of the digital elevation model was 4 m. Gridding of the data was carried out using the inverse distance-weighted method. Similar interpolation methods were used for creating surfaces of the spatial distribution of magnetic measurements and metal concentrations. Buffer zones of variable distances were used to calculate the proximity of the particular topographic features from areas exhibiting high magnetic values or heavy metal concentrations.

Results

Magnetic susceptibility (χ), anhysteritic remanent magnetization (ARM) and the isothermal remanent magnetization (IRM) are all concentration parameters. The magnetic susceptibility (χ) is usually proportional to the concentration of ferromagnetic oxides (such as magnetite and maghemite), while ARM and IRM values are more highly affected by magnetite grain size variations and by antiferromagnetic components (e.g. hematite and goethite) than is susceptibility (Walden et al. 1999).

The distribution of the low field magnetic susceptibility and the frequency-dependent susceptibility is presented in Fig. 5. High susceptibility values are generally oriented NW–SE, while increased values of the frequency-dependent susceptibility are mainly distributed in the northeastern part of the study area.

According to Pearson's coefficient (Table 1), a strong relation is obtained between SIRM–χ, SIRM–ARM and χ–ARM. The content of ferromagnetic minerals, produced by the lignite process, decreases toward the bottom left corner of the diagram of Fig. 6a. Samples in the lower part of the diagram are characterized by low SIRM and susceptibility and they were collected from areas situated away from the quarries and depositories. Their behavior suggests a dominant paramagnetic mineral content. Samples characterized by low to moderate SIRM and moderate χ come from areas situated near to depositories and parallel

Fig. 4 Details from the Megalopolis power plant (above) and its surrounding lignite mines (below)

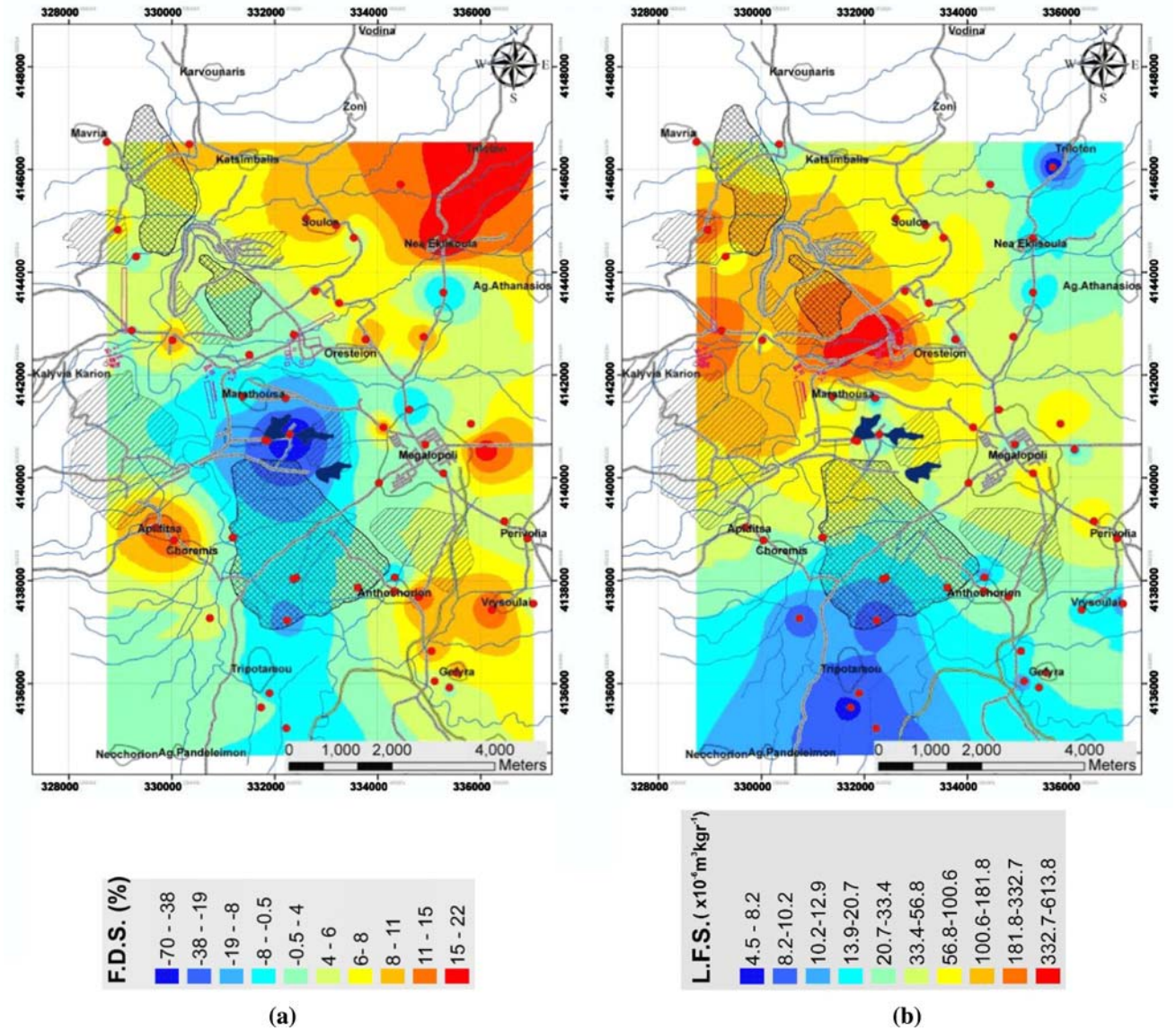

Fig. 5 Mapping of (**a**) frequency-dependent susceptibility (F.D.S.) and (**b**) low field magnetic susceptibility (L.F.S.)

to the orientation of the wind currents. Data displayed in the upper part of the diagram correspond to moderate–high SIRM and χ indicating samples with considerable contributions of coarse ferromagnetic grains. The particular samples were collected from active quarries and depositories. Similarly, plots of ARM versus χ and ARM versus SIRM (Fig. 6b, c) clearly distinguish two different groups of samples, one with samples from within and near the quarries and another with samples located away from them.

IRM measurements can be informative also for the magnetic carrier of the samples. The shape of the IRM curve indicated the presence of magnetite in most of the samples. Nevertheless, more detailed analysis of the curves proved to be successful in finding some differences between the two groups of samples. Samples of the first group (in the vicinity of the quarries) indicated that 90% of the magnetic minerals in their structure are of ferrimagnetic nature (such as magnetite and maghemite) and they saturate up to 300 mT (Fig. 7a). On the other hand, samples from the second group (away from the lignite quarries) seem to have a second strong magnetic component, which is not saturated up to 1,200 mT, suggesting the presence of hematite or goethite. These minerals are common in natural soils, indicating that these samples are not polluted (Fig. 7b). IRM analysis was performed with IRM-CLG software package of Kruiver et al. (2001). Additionally, thermomagnetic analysis (Fig. 8) confirmed the presence of magnetite as a main magnetic mineral in the samples of the first groups and the contribution of hematite in the samples of the second group.

Table 1 Pearson's coefficients for both magnetic properties and heavy metal concentrations

	K	CA	TI	MN	FE	NI	CU	ZN	PB	RB	SR	Y	ZR	NB	sus-I (χ)	sus-h	f.d. sus	ARM	SIRM	SIRM/χ	ARM/χ
K	–	−0.23	0.40	−0.10	0.25	0.62	0.45	0.24	0.24	0.85	−0.01	0.48	−0.07	0.29	−0.05	−0.05	−0.08	0.00	0.04	0.05	−0.49
CA		–	−0.46	−0.25	−0.25	−0.33	−0.07	−0.02	−0.09	−0.52	0.72	−0.76	−0.74	−0.64	−0.03	−0.04	0.15	0.01	0.00	−0.24	−0.47
TI			–	0.07	−0.05	0.30	−0.09	−0.01	0.19	0.60	−0.37	0.63	0.47	0.71	−0.35	−0.35	−0.04	−0.38	−0.40	0.04	0.28
MN				–	0.32	−0.16	0.03	0.05	0.08	−0.05	−0.29	0.05	0.31	0.13	0.31	0.31	0.37	0.38	0.41	−0.16	−0.01
FE					–	0.31	0.36	0.01	0.03	0.39	−0.07	0.32	0.00	0.30	0.77	0.77	−0.04	0.92	0.94	0.20	−0.04
NI						–	0.69	0.12	0.02	0.75	−0.04	0.63	−0.10	0.24	0.02	0.03	−0.15	0.21	0.21	0.06	−0.54
CU							–	0.35	0.27	0.46	0.19	0.39	−0.16	0.09	0.33	0.33	−0.05	0.45	0.47	0.16	−0.58
ZN								–	0.64	0.08	0.00	−0.02	−0.12	−0.22	0.02	0.02	0.02	−0.10	−0.07	0.19	−0.25
PB									–	0.12	−0.08	0.09	0.10	0.08	0.00	0.00	0.15	−0.15	−0.16	−0.07	−0.05
RB										–	−0.19	0.79	0.20	0.63	0.00	0.00	−0.20	0.12	0.16	0.20	−0.34
SR											–	−0.37	−0.56	−0.29	0.13	0.13	0.15	0.17	0.17	−0.09	−0.28
Y												–	0.59	0.78	0.04	0.05	−0.23	0.07	0.06	0.36	0.12
ZR													–	0.60	−0.03	−0.03	0.05	−0.12	−0.17	−0.04	0.87
NB														–	0.08	0.08	−0.13	0.30	0.28	0.16	0.39
sus-I (χ)															–	1.00	0.05	0.99	0.98	0.20	−0.05
sus-h																–	0.04	0.99	0.99	0.21	−0.05
f.d. sus																	–	0.08	0.06	−0.73	0.16
ARM																		–	0.99	0.20	0.05
SIRM																			–	0.27	−0.22
SIRM/sus-I																				–	−0.02
ARM/sus-I																					–

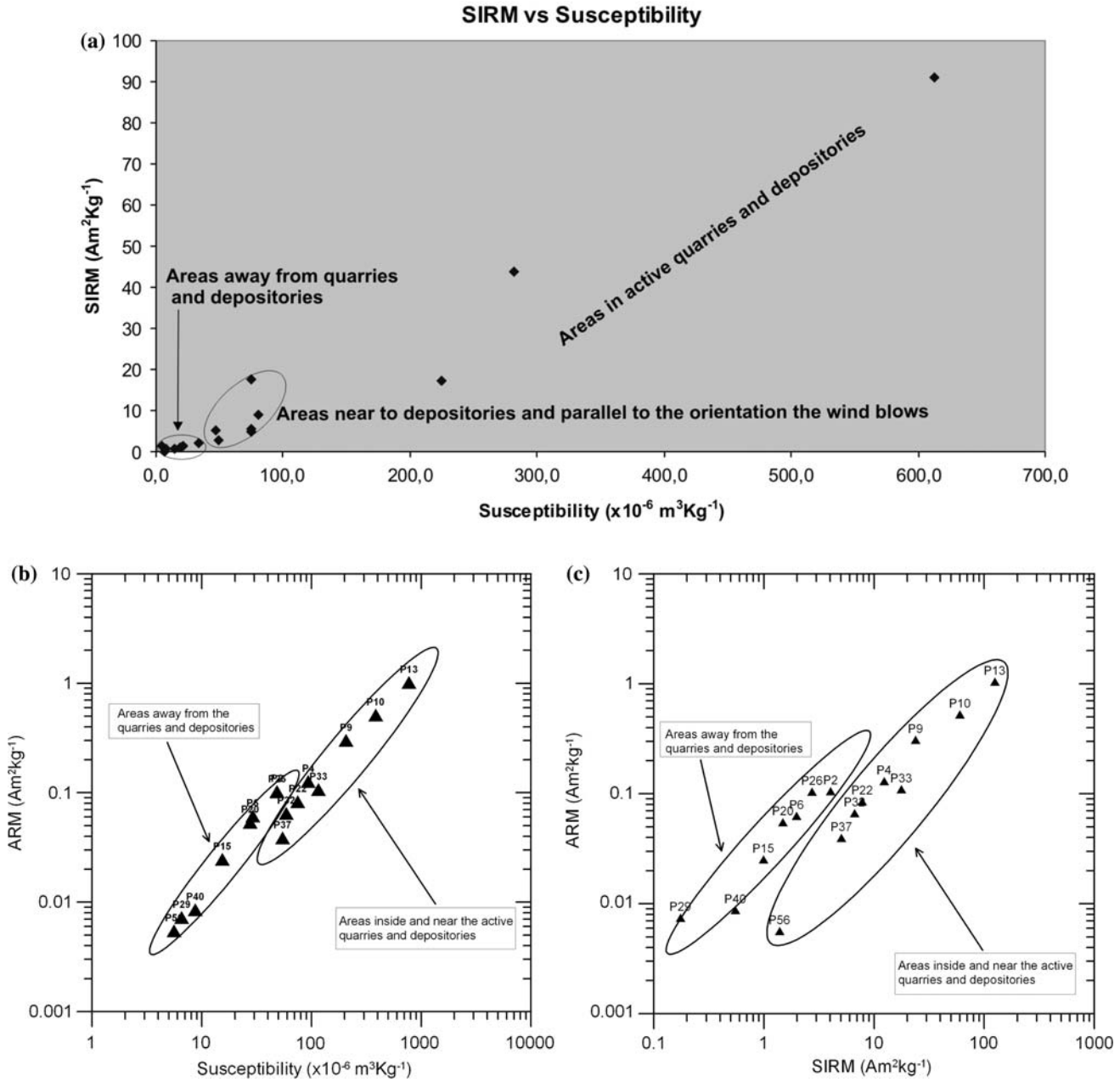

Fig. 6 Plots of (**a**) SIRM versus susceptibility, (**b**) ARM versus susceptibility, (**c**) ARM versus SIRM

Table 1 shows the Pearson's coefficients among metal concentrations and magnetic properties. Pearson's coefficients were determined taking into account all samples analyzed. The correlation among magnetic properties is very high confirming the reliability of the applied methods. Additionally, the overall correlation of χ and metals is strong for Fe, while for the cases of Ti, Mn and Cu a weak relation is suggested. Actually, the highest values of χ, Fe and Rb are noticed in the area of the Power Plant. We have to refer that this relation changes in case we take into account the altitude of the study area, namely the relation between χ and Ti, Mn, Cu becomes stronger for low-altitude areas. In contrast, there is no linear relation between the majority of metals and frequency-dependent (f.d.) susceptibility. The only exception is the case of Mn, which shows a weak correlation taking into account the entire study area, but a strong relation for the low relief regions (both the f.d. susceptibility and Mn exhibit a minimum value in the area of the lakes at the lowest relief of the region). ARM/χ shows a strong relation to Zr and a moderate relation to K, Ca, Ni and Cu concentrations.

The correlations among the metals are also confirmed by the observed patterns presented on the distribution maps of Fig. 9. A strong relation is shown between K–Rb, Ni–Rb,

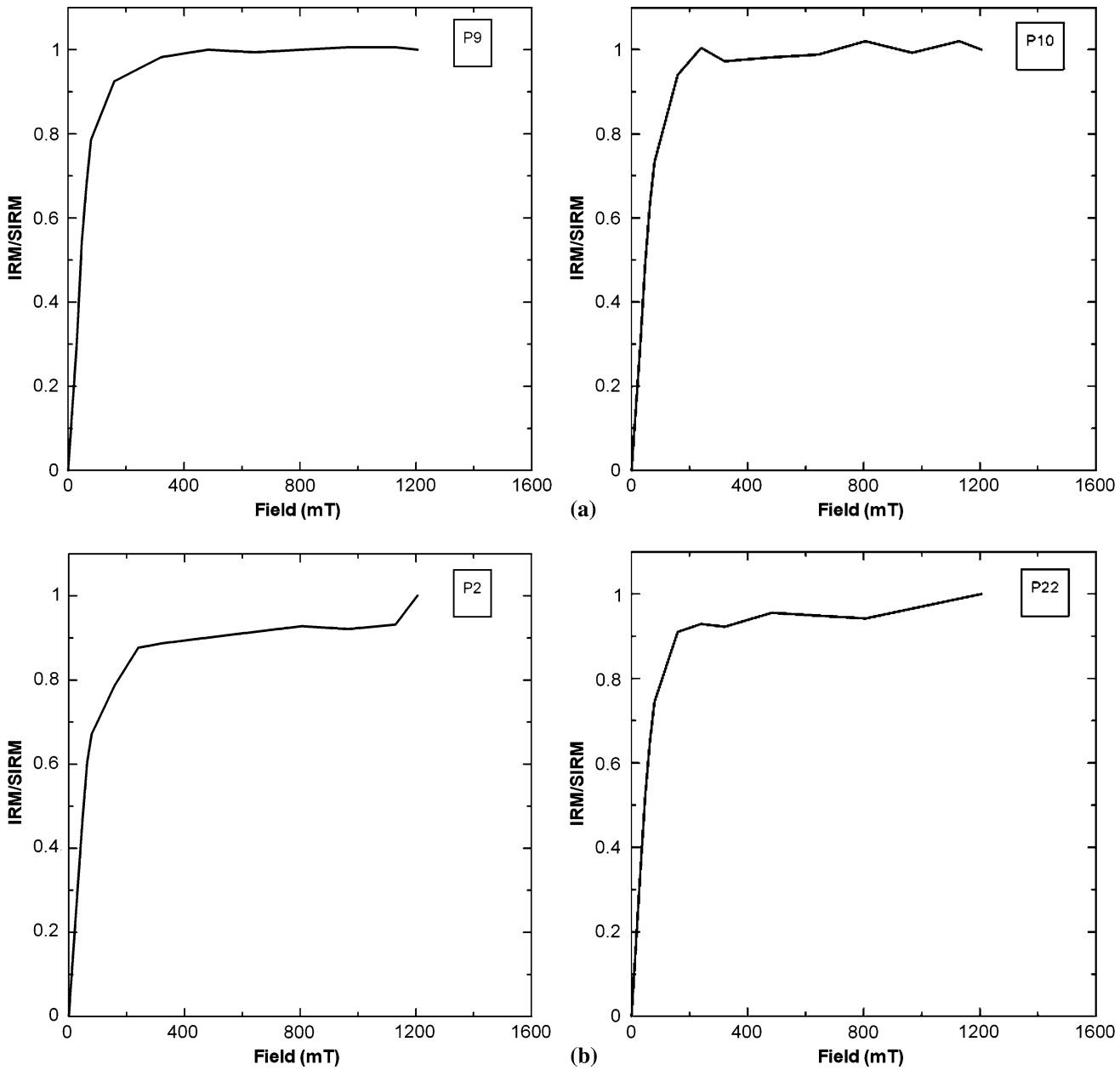

Fig. 7 Indicative IRM curves from selected samples (P9 and P10), which are located inside the quarries (**a**) and samples (P2 and P22), which are far away from the quarries and the depositories (**b**)

Rb–Y and Y–Nb concentrations. A moderate relation is indicated between K–Ni, Ca–Rb, Ca–Sr, Ca–Zr, Ca–Nb, Ti–Rb, Ti–Y, Ti–Nb, Ni–Cu, Ni–Y, Zn–Pb, Rb–Nb and Y–Zr concentrations (see Pearson's coefficients in Table 1).

Discussion and conclusions

At first sight in Table 1, no relation between Fe and the rest of the metals is detected. This is because the majority of the samples were taken into account. A more detailed observation of the soil samples suggests that there is a strong relation between the geological structure of the study area and the distribution of the metals. Figure 10 shows the relation between Fe concentration and Ni, K, Rb and Y, using samples collected from sites filled by sediments older than Pleistocene. In the particular analysis, samples collected from the quarries or the depositories were excluded, since the sediments are severely disturbed in these locations. The linear correlation factors between Fe–Ni, Fe–K, Fe–Rb and Fe–Y are 0.75, 0.7, 0.85 and 0.68, respectively. Generally low correlation between Fe

concentration and the rest of metals has been determined for the samples collected from sites filled by Holocene sediments. The SIRM values of Pleistocene and older sediments located away from the quarries and the depositories vary in the range 2.34–17.7 A m^2 kg^{-1}, while Holocene sediments correspond to values lower than 2.0 A m^2 kg^{-1}. We strongly believe that there is also a strong relation between the orientation of the drainage network and Fe, Ni, Cu, Rb, Y concentrations. The drainage network is dense in the western part of the study area where the concentrations of Fe, Ni, Cu, Rb and Y are locally high. Additionally, the high values of f.d. susceptibility show an NW–SE orientation trend, which coincides with the orientation of Mn high concentrations. It is also possible that the above trends have been influenced by the NW–SE orientation of the wind currents in the study area.

The main transmission factors in the study area are the drainage network and the wind. High values of the magnetic susceptibility χ are orientated along NW–SE, which is the orientation in which the wind blows. Low values of the magnetic susceptibility χ are mainly distributed in the southern part of the study area, even though the drainage network is also well developed in this part of the study area. The reason for the low magnetic susceptibility values in this area is the flow orientation of the drainage network, i.e. the rain water is carried away from the southeastern to northwestern part of the valley. Magnetic properties of the examined soil samples agree that the metal pollution reveals high values around the quarries and depositories and is generally orientated along a NW–SE direction. Additionally, the pollution is transmitted NW out of the Megalopoli's basin due to the drainage network. High linear correlation factors were observed between Fe and Ni, K, Rb, Y concentrations, respectively, in sediments older than Pleistocene, indicating the relation of the geologic features with the specific metals.

Finally, the spatial distribution of the above attributes indicated that the highest values in Pb, Zn and Mn exist in the area of Megalopolis town, followed by Apiditsa and Choremis villages, the later indicating also high Br values.

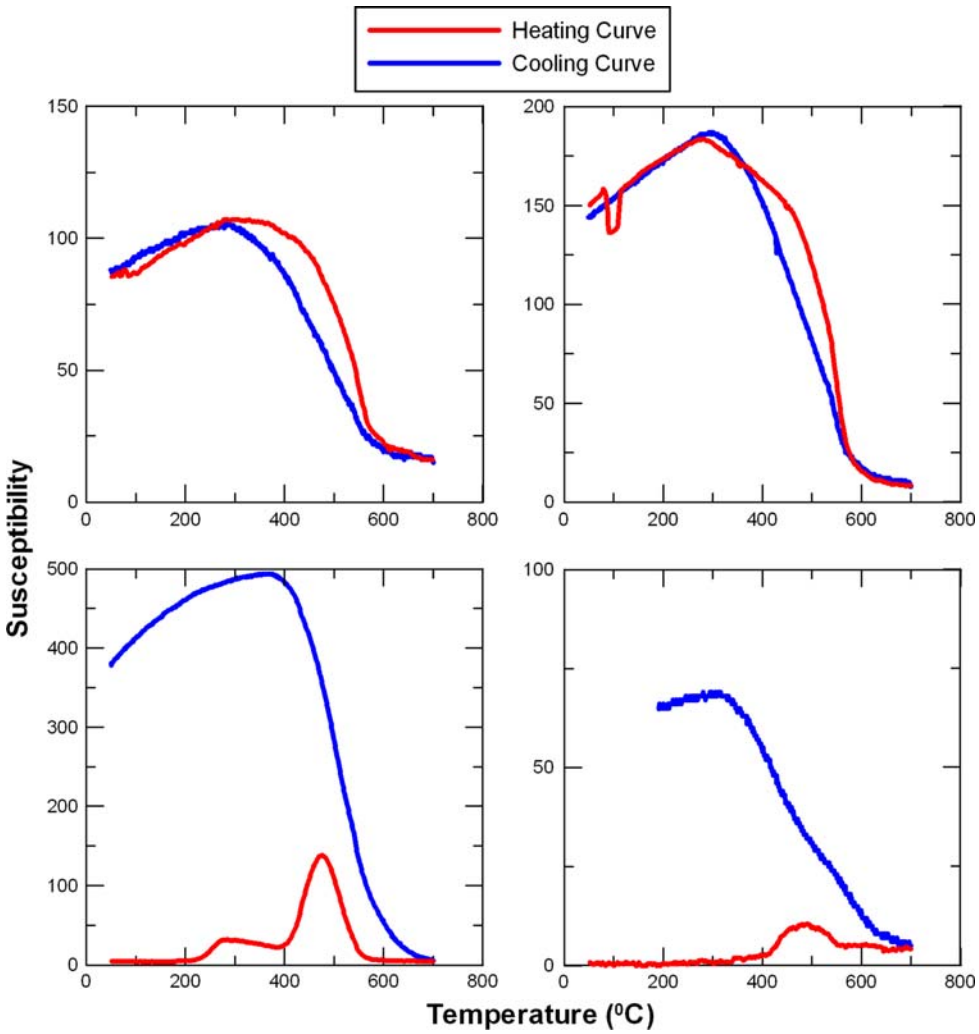

Fig. 8 Thermomagnetic curves of samples of Fig. 6. Samples, which are located inside the quarries (*upper part*), indicate the presence of magnetite. Samples, which are far away from the quarries and the depositories (*lower part*), show additional small contribution of hematite

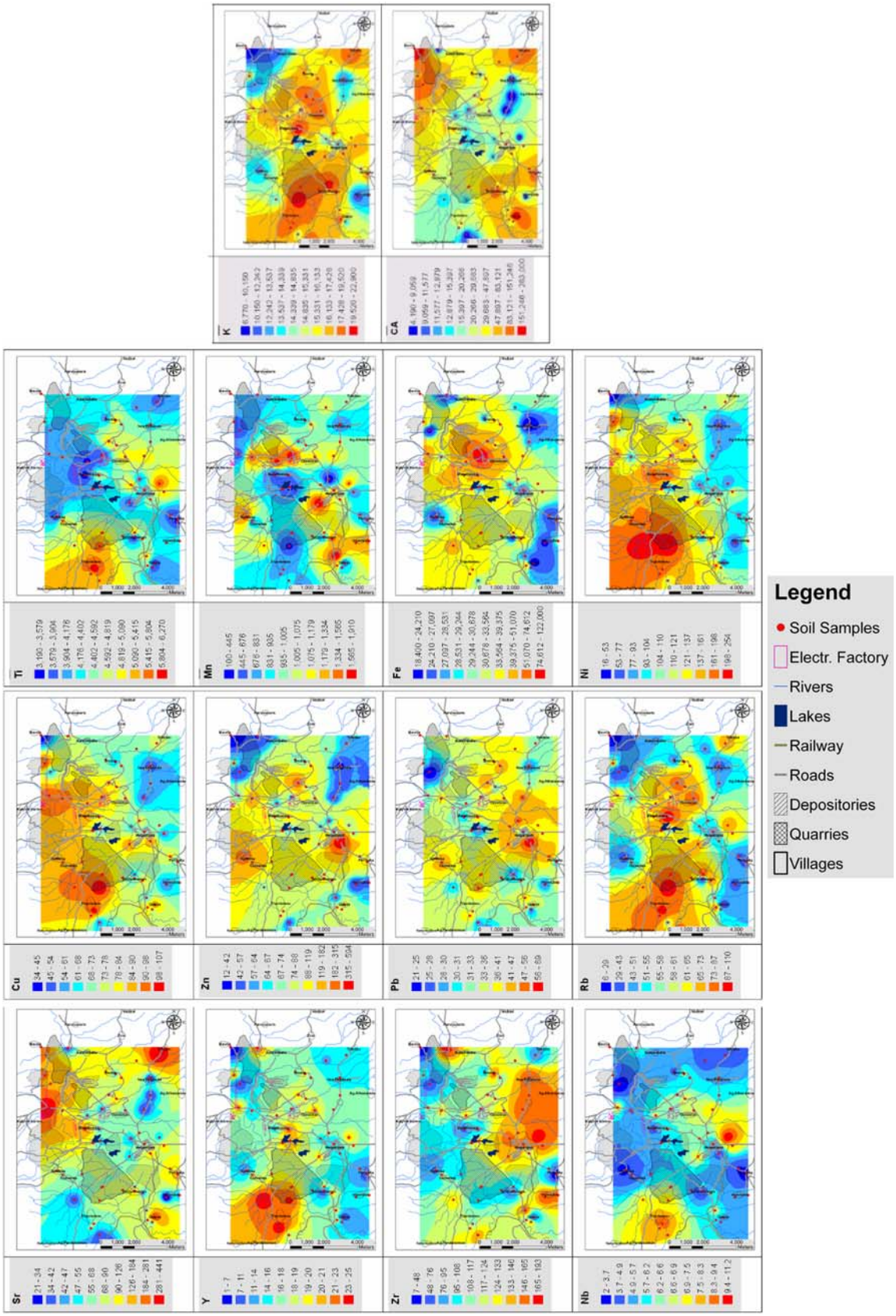

Fig. 9 Mapping heavy metals concentrations (in ppm)

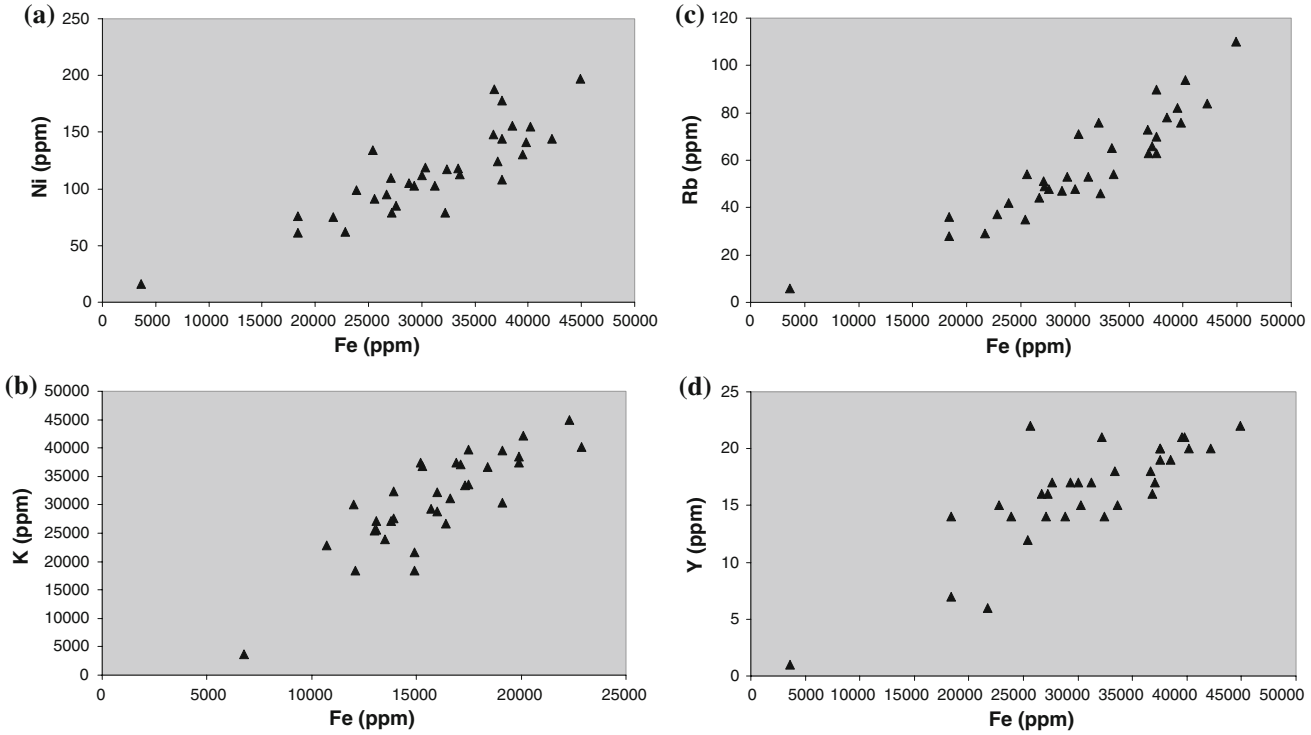

Fig. 10 Mapping of Fe concentration versus (**a**) Ni, (**b**) K, (**c**) Rb and (**d**) Y for the samples collected from sediments older than Pleistocene located out of the quarries and depositories

High values of Nb and Zr were shown in the vicinity of Megalopolis. The vicinity of Tripotamou village presents high values of Cu, Ti, Nb, Y and Rb. On the other hand, high levels of Sr are indicated close to Trilofon and Gefyra villages. Actually, the vicinity of all the above villages exhibits high f.d. susceptibility values.

The results of our investigation generally confirm that magnetic susceptibility measurements provide the basis for an environmental study in polluted areas. Furthermore, the terrain attributes seem to play also an important role in the distribution of the heavy metals and for this reason GIS techniques provide an excellent tool for studying the spatial distribution and relation between magnetic susceptibility, heavy metal concentrations and the natural settings of a study area.

As future work, we plan to extend the above methodology in the area located to the north of the study area, to investigate the role of the drainage network as a transmission factor of the metal pollution.

Acknowledgments We are grateful to the Public Power Corporation (DEI) for providing the topographic data and information for the study area. Special thanks also to Prof. R. Scholger for his valuable suggestions and for allowing us to carry out the ARM measurements in the Palaeomagnetic Laboratory Gams of Leoben University in Austria. We wish to thank Dr. Sultan Awad Sultan Araffa and an anonymous reviewer for their constructive criticism, which improved a version of this manuscript.

References

Beckwith PR, Ellis JB, Revitt DM, Oldfield F (1984) Identification of pollution sources in urban drainage systems using magnetic methods. In: Balmer P, Malmqvist PA, Sjoberg A (eds) Proceedings of the third international conference on urban storm drainage, Göteborg, Sweden, June 4–8, 1984, pp 1313–1322

Bityukova L, Scholger R, Birke M (1999) Magnetic susceptibility as indicator of environmental pollution of soils in Tallinn (Estonia). Phys Chem Earth 24:829–835

Boyko T, Scholger R, Stanjek H, MAGPROX Team (2004) Topsoil magnetic susceptibility mapping as a tool for pollution monitoring: repeatability of in situ measurements. J Applied Geophys 55:249–259

Dearing JA, Hannam JA, Anderson AS, Wellington EMH (2001) Magnetic, geochemical and DNA properties of highly-magnetic soils in England. Geophys J Int 144:183–196

Dekkers MJ (1997) Environmental magnetism: an introduction. Geol Mijnbouw 76:163–182

Dekkers M, Pietersen HS (1992) Magnetic properties of low-Ca fly ash: a rapid tool for Fe-assessment and a survey for potentially hazardous elements. Mater Res Soc Symp Proc 245:37–47

Flanders PJ (1994) Collection, measurement and analysis of airborne magnetic particulates from pollution in the environment. J Appl Geophys 75:5931–5936

Flanders PJ (1999) Identifying fly ash at a distance from fossil fuel power stations. Environ Sci Technol 33:528–532

Fountoulis IG (2000) Neotectonic evolution of the Central–western Peloponnessos. PhD Thesis, National and Kapodistrian University of Athens, Greece

Goluchowska BJ (2001) Some factors affecting an increase in magnetic susceptibility of cement dusts. J Appl Geophys 48:103–112

Hanesch M, Scholger R, Rey D (2003) Mapping dust distribution around an industrial site by measuring magnetic parameters of tree leaves. Atmos Environ 37:5125–5133

Hansen LD, Silberman D, Fisher GL (1981) Crystalline components of stack-collected, size-fractionated coal fly ash. Environ Sci Technol 15:1057–1062

Heller F, Strzyszcz Z, Magiera T (1998) Magnetic record of industrial pollution in forest soils of Upper Silesia, Poland. J Geophys Res 103/B8:767–774

Hoffmann V, Knab M, Appel E (1999) Magnetic susceptibility mapping of roadside pollution. J Geochem Explor 66:313–326

Jordanova NV, Jordanova DV, Veneva L, Yorova K, Petrovsky E (2003) Magnetic response of soils and vegetation to heavy metal pollution—a case study. Environ Sci Technol 37:4417–4424

Kapička A, Petrovskỳ E, Ustjak S, Machačkova K (1999) Proxy mapping of fly-ash pollution of soils around a coal burning power plant: a case study in the Czech Republic. J Geochem Explor 66:291–297

Kokinou E, Saltas V, Kavousanakis M, Egglezou ME, Vallianatos F (2008) Magnetic susceptibility mapping of the municipal park of Chania (Crete, Greece). In: Proceedings of the 2nd international workshop on geoenvironment and geotechnics (GEOENV), Milos Island, Greece, September 2008, pp 131–135

Kruiver PP, Dekkers MJ, Heslop D (2001) Quantification of magnetic coercivity components by the analysis of acquisition curves of isothermal remanent magnetisation. Earth Planet Sci Lett 189:269–276

Lecoanet H, Leveque F, Segura S (1999) Magnetic susceptibility in environmental applications: comparison of field probes. Phys Earth Planet Inter 115:191–204

Lecoanet H, Leveque F, Ambrosi JP (2001) Magnetic properties of salt-marsh soils contaminated by iron industry emissions (Southeast France). J Appl Geophys 48:67–81

Petrovský E, Ellwood BB (1999) Magnetic monitoring of air-, land- and water pollution. In: Maher BA, Thompson R (eds) Quaternary climates, environments and magnetism. Cambridge University Press, Cambridge, pp 279–322

Petrovsky E, Kapička A, Jordanova N, Borůvka L (2001) Magnetic properties of alluvial soils contaminated with lead, zinc and cadmium. J Appl Geophys 48:127–136

Riga-Karandinos AN, Karandinos MG (1998) Assessment of air pollution from a lignite power plant in the plain of Megalopolis (Greece) using as biomonitors three species of lichens; impacts on some biochemical parameters of lichens. Sci Total Environ 215(1/2):167–183

Romic M, Hengl T, Romic D, Husnjak S (2007) Representing soil pollution by heavy metals using continuous limitation scores. Comput Geosci 33(10):1316–1326

Sarris A, Galaty ML, Yerkes RW, Parkinson W, Gyucha A, Billingsley DM, Tate R (2004) Geophysical prospection and soil chemistry at the Early Copper Age settlement of Veszto-Bikeri, Southeastern Hungary. J Archaeol Sci 31(7):927–939

Schmidt A, Yarnold R, Hill M, Ashmore M (2005) Magnetic susceptibility as proxy for heavy metal pollution: a site study. J Geochem Explor 85:109–117

Scholger R (1998) Heavy metal pollution monitoring by magnetic susceptibility measurements applied to sediments of the river Mur (Styria, Austria). Eur J Environ Eng Geophys 3:25–37

Sharma PA, Tripathi BD (2008) Magnetic properties of fly ash pollution and heavy metals from soil samples around a point source in a dry tropical environment. Environ Monit Assess 138(1–3):31–39

Strzyszcz Z, Magiera T, Heller F (1996) The influence of industrial emissions on the magnetic susceptibility of soils in Upper Silesia. Stud Geophys Geod 40:276–286

Sukumar A, Subramanian R (2003) Elements in the hair of non-mining workers of a lignite open mine in Neyveli. Ind Health 41(2):63–68

Thompson T, Oldfield F (eds) (1986) Environmental magnetism. Allen and Unwin, London

Vassilev S (1992) Phase mineralogy studies of solid waste products from coal burning at some Bulgarian thermoelectric power plants. Fuel 71:625–633

Verosub KL, Roberts AP (1995) Environmental magnetism: past, present, and future. J Geophys Res 100:2175–2192

Yerkes R, Sarris A, Frolking T, Parkinson W, Gyucha A, Hardy M, Catanoso L (2007) Geophysical and geochemical investigations at two early Copper Age settlements in the Koros river valley, Southeastern Hungary. Geoarchaeology 22(8):845–871

Walden J, Oldfield F, Smith J (1999) Environmental magnetism: a practical guide. Technical guide, no. 6. Quaternary Research Association, London

Wang XS, Qin Y (2005) Correlation between magnetic susceptibility and heavy metals in urban topsoil: a case study from the city of Xuzhou, China. Environ Geol 49(1):10–18

Zeneli L, Daci NM, Daci-Ajvazi MN, Paçarizi H (2008) Effects of pollution on lead and cadmium concentration and correlation with biochemical parameters in blood of human population nearby Kosovo thermo power plants. Am J Biochem Biotechnol 4(3):273–276